Available online at www.sciencedirect.com

SciVerse ScienceDirect

Ceramics International 39 (2013) 4609–4617

CERAMICS INTERNATIONAL

www.elsevier.com/locate/ceramint

Defect-induced room temperature ferromagnetism in B-doped ZnO

S. Yılmaz[a,b,*], J. Nisar[c], Y. Atasoy[a], E. McGlynn[b], R. Ahuja[c,d], M. Parlak[e], E. Bacaksız[a]

[a]Department of Physics, Faculty of Sciences, Karadeniz Technical University, 61080 Trabzon, Turkey
[b]School of Physical Sciences and National Center for Plasma Science and Technology, Dublin City University, Glasnevin, Dublin 9, Ireland
[c]Condense Matter Theory Group, Department of Physics and Astronomy, Box 516, Uppsala University, 751 20 Uppsala, Sweden
[d]Applied Materials Physics, Department of Materials and Engineering, Royal Institute of Technology (KTH), S-100 44 Stockholm, Sweden
[e]Department of Physics, Middle East Technical University, 06531 Ankara, Turkey

Received 5 October 2012; received in revised form 12 November 2012; accepted 21 November 2012
Available online 27 November 2012

Abstract

ZnO microrods were grown on glass substrates by the spray pyrolysis method and boron was doped into the ZnO microrods by diffusion. X-ray diffraction results confirmed that the incorporation of B leads to a slight reduction in the deposit texture. Scanning electron microscopy measurements showed that the morphology of the ZnO samples changed from a microrod to nanocrystalline structure with B-doping. Photoluminescence data indicate that B-doping leads to a relative increase of the unstructured green band intensity. Magnetic measurements revealed that B-doped ZnO samples exhibited room temperature ferromagnetism related to defects, in agreement with first principles theoretical calculations.
© 2012 Elsevier Ltd and Techna Group S.r.l. All rights reserved.

Keywords: ZnO:B; Photoluminescence; Ferromagnetism; First-principle calculation

1. Introduction

ZnO has attracted great interest because it has a direct band gap of 3.37 eV at room temperature and a large excitonic binding energy of 60 meV. By combining these optical properties with its electrical properties, ZnO has many important potential applications in the field of electro-optical devices such as UV light emitters, transparent electrodes, gas sensors and solar cells [1–3]. ZnO has also a ubiquitous intrinsic n-type electrical conductivity, which is attributed to various intrinsic defects like oxygen vacancies and zinc interstitials as well as extrinsic impurities such as hydrogen and other impurities. After doping by group III elements such as B, Al and Ga, which act as donors in ZnO, the electrical properties of ZnO can be altered and controlled [4,5].

ZnO has received considerable attention since Dietl et al. [6] theoretically predicted that ZnO should be a good candidate for room temperature Dilute Magnetic Semiconductors (DMS) for spintronic applications. After this theoretical study, many research groups have reported studies on transition-metal (TM)-doped ZnO exhibiting ferromagnetism with a T_c above room temperature. For example, Ueda et al. [7] obtained ferromagnetic behavior with a Curie temperature higher than room temperature for Co-doped ZnO films grown by the pulsed laser deposition method. Additionally, Liu et al. [8] reported room temperature ferromagnetism in Ni-doped ZnO thin films also grown by the pulsed-laser deposition method. The work by Pradhan et al. [9] indicated that $Zn_{1-x}Mn_xO$ films grown at a substrate temperature of 500 °C exhibited room temperature ferromagnetism and growths beyond 500 °C showed a decrease in the magnetization due to the formation of Mn-related clusters.

In recent years, many experimental and computational groups have focused on examining the influence of non-magnetic ion doping (C, In, N and B) in ZnO to obtain high T_c ferromagnetic semiconductor. For instance, Pan et al. [10] predicted ferromagnetic behavior with a T_c over 400 °C in C-doped ZnO based on their first-principles calculations. Specifically they predicted a magnetic moment of 2.02 μ_B per carbon atom as carbon substituted oxygen in ZnO. This theoretical prediction was later confirmed experimentally

*Corresponding author at: Department of Physics, Faculty of Sciences, Karadeniz Technical University, 61080 Trabzon, Turkey.
Tel.: +90 462 377 25 53; fax: +90 462 325 31 95.
E-mail address: slh_yilmaz@yahoo.com.tr (S. Yılmaz).

0272-8842/$ - see front matter © 2012 Elsevier Ltd and Techna Group S.r.l. All rights reserved.
http://dx.doi.org/10.1016/j.ceramint.2012.11.060

for the C-doped ZnO films grown by the pulsed laser deposition method. Ye et al. [11] studied C-doped ZnO powder samples prepared by a standard solid state reaction method and sintered separately in both argon and nitrogen ambient that showed ferromagnetic behavior at room temperature. However, the samples grown in an argon atmosphere had a larger ferromagnetism than those grown in nitrogen. Liu et al. [12] obtained room temperature ferromagnetic behavior for their In-doped ZnO nanowires, showing that the ferromagnetism enhanced significantly with In-doping and they explained that the origin of the observed ferromagnetism is related to oxygen vacancies induced by In-doping. Furthermore, the study reported by Wu et al. [13] indicated that N-doped ZnO thin films synthesized by pulsed laser deposition method under different N_2 pressures exhibiting room temperature ferromagnetism. They clarified that the origin of ferromagnetism of the samples of ZnO:N grown under a pressure of 10 Pa is attributed to Zn interstitial defects. However, Zn vacancy defects were attributed as the cause of ferromagnetism in samples of ZnO:N grown under a pressure of 50 Pa. Xu et al. [14] obtained room temperature ferromagnetism experimentally following their theoretical predictions of such behavior for their B-doped ZnO thin films prepared by the pulsed laser deposition technique. They explained that the origin of the ferromagnetism in their samples is due to the induced magnetic moment of oxygen atoms in the nearest neighbor sites to B–Zn vacancy pairs. Therefore, although there are many experimental studies on magnetic and non-magnetic doped ZnO showing room temperature ferromagnetism, there is no consensus on the origin of ferromagnetism in doped ZnO-based materials [15–17]. The origin of the ferromagnetism in nonmagnetic ion-doped ZnO is very likely to be significantly different from that in the case of TM-doped ZnO due to the dominant *p–p* interactions in the former rather than the *d–d* and *p–d* interactions in the latter [18]. However, recent studies on both magnetic and non-magnetic ion-doped ZnO proposed that intrinsic defects also are very important in terms of their contribution to ferromagnetic ordering in oxide based DMS [19,20].

To our knowledge, there are few reports in the literature on B-doped ZnO microrods, especially in terms of investigation of the magnetic properties of these samples in conjunction with other sample properties. In this paper, we have studied the structural, optical, electrical and magnetic properties of B diffusion-doped ZnO (ZnO:B) samples, which were synthesized via a spray pyrolysis method on glass substrates and diffusion-doped at 600 °C for different annealing times under an argon ambient atmosphere. We have studied the effects of B diffusion-doping on intrinsic defects using photoluminescence and we have also tried to correlate the optical and magnetic properties to explain the origin of the observed room temperature ferromagnetism in our samples. In addition, first principles theoretical calculations were made to further clarify the origin of the observed ferromagnetism and to complement the deductions from the experimental measurements.

2. Experimental and computational details

ZnO microrod arrays were prepared by the spray pyrolysis method in an air atmosphere. The experimental setup and other experimental procedures are explained in more detail elsewhere [21]. The solution was prepared from zinc chloride ($ZnCl_2$) at 0.1 M concentration in deionized water and was then sprayed on the glass substrates. The growth was performed with a spray rate of ~5 ml/min and a growth rate of ~50 nm/min. Prior to growth, the glass substrates were cleaned in ethanol and then dried in vacuum. During the growth, the substrates were rotated with a speed of 10 revolutions per minute and the substrate was held at a temperature of 550 °C. Boron metal was evaporated on deposited ZnO microrods by an e-beam evaporation system with a pressure during deposition of $\sim 6 \times 10^{-6}$ Torr. The amount of B deposited was measured by spectroscopic ellipsometry (Angstrom Advanced Inc., model PHE 102) and found to be ~20 nm. After B deposition, the samples were annealed in a one side sealed quartz tube which was first evacuated to $\sim 10^{-3}$ Torr and then filled with high purity argon gas to a pressure of $\sim 1.5 \times 10^{+3}$ Torr for the actual annealing procedure. Annealing of the samples was carried out a fixed temperature of 600 °C for 8, 16 and 24 h durations. The crystal structure of the samples was investigated using a Bruker AXS D8 advance texture diffractometer with CuK_α radiation, operated at a voltage of 40 kV and a current of 40 mA, over the range $2\theta = 20$–60° with a step of 0.01° at room temperature. The crystal quality was further studied by X-ray rocking curve (XRC) measurements of the (002) reflection over the range $\omega = 0$–30° with a step of 0.01°. The surface morphology was studied with a Zeiss EVOLS 15 SEM (scanning electron microscopy) with an acceleration voltage of 20 kV. The resistivity and carrier concentration of the samples were determined, respectively, by four point probe and Hall Effect measurements. For this, a Keithley, model 2400 series sourcemeter was used to measure the required parameters with a home-made system using a four probe configuration at room temperature. The detailed chemical composition and bonding types in the surface and near-surface regions of the deposits were examined by X-ray photoelectron spectroscopy (XPS) using an UNISPECS ESCA system equipped with an Al Kα X-ray radiation source of 1486.6 eV-energy. The kinetic energies of emitted electrons from the samples were analyzed by a concentric hemispherical analyzer, which operates in the constant pass-energy (CAE) mode, under a vacuum of $\sim 1 \times 10^{-9}$ Torr. The surface of the as-grown samples was sputtered by argon ions before XPS in order to clean the surfaces and avoid contributions from unintentionally deposited C and O contamination due to atmospheric exposure. To correct for any charging effects, the adventitious carbon C 1s photoelectron peak at 285.0 eV was consistently used as a reference for the binding energies of core levels and Auger peaks. Photoluminescence (PL) measurements were performed at 10 K,

using a SPEX 1704 monochromator and the samples were cooled with a closed cycle cryostat (model Janis SHI-950-5). PL spectra were excited with the 325 nm line of a He–Cd laser operating at 20 mW, unfocussed on the sample surface. Magnetization measurements of the samples as a function of magnetic field and temperature were carried out using a Quantum Design Physical Property Measurement System (PPMS) with a vibration sample magnetometer module.

The first-principles theoretical calculations were carried using a projected augmented wave (PAW) method [22] as implemented in the Vienna ab-initio simulation package (VASP) [23,24]. The generalized gradient approximation (GGA-PBE) [25,26] was used for the exchange-correlation potential. A plane-wave cutoff energy of 500 eV is used throughout the calculations. In all calculations, self-consistency is achieved with a tolerance in the total energy of at least 0.1 meV and a Gaussian smearing width of 0.1 eV is used. PAW potentials with the valence states 4 s and 3d for Zn, 2s and 2p for O, B were employed. A gamma-centered k-mesh was used to sample the irreducible Brillioun zone (IBZ) [27]. A k-points mesh of $3 \times 3 \times 3$ was found to be sufficient to reach convergence for bulk calculations.

3. Results and discussion

Fig. 1(a)–(d) shows the XRD data for undoped ZnO annealed at 600 °C and B diffusion-doped ZnO microrod samples annealed at 600 °C for 8, 16 and 24 h in argon, respectively. The observed reflections from these samples are in good agreement with the JCPDS standard data (PDF No. 36-1451) of wurtzite (hexagonal) ZnO powder. It was seen that both undoped and B diffusion-doped ZnO samples exhibit peaks corresponding to the (002), (101) and (102) planes, with the (002) peak showing by far the highest intensity in all cases, implying that all the samples have a hexagonal crystal structure with a preferred orientation (texture) with the substrate normal parallel to the normal to the ZnO (002) plane. No peaks belonging to B and its oxides or other impurity phases were detected within the sensitivity of our XRD measurements, indicating that the B was incorporated into the ZnO host lattice without changing the crystal structure and orientation. The *c*-axis lattice parameter value is calculated using the ZnO (002) reflection and it is found that undoped ZnO sample annealed at 600 °C show a dominant peak at about 34.35° corresponding to a *c*-axis lattice parameter value of 0.522 nm. However, the reflections from B diffusion-doped ZnO microrods were shifted to larger angles, implying that *c*-axis lattice parameter values decreased with increased annealing time as listed in Table 1. The reduction of the lattice parameter value is probably due to the substitution of lower radii of B^{3+} (0.027 nm) with higher radii of Zn^{2+} (0.074 nm). The decrease of the *c*-axis lattice parameter upon B incorporation indicates that the samples were in a state of compressive strain along the *c*-axis [28].

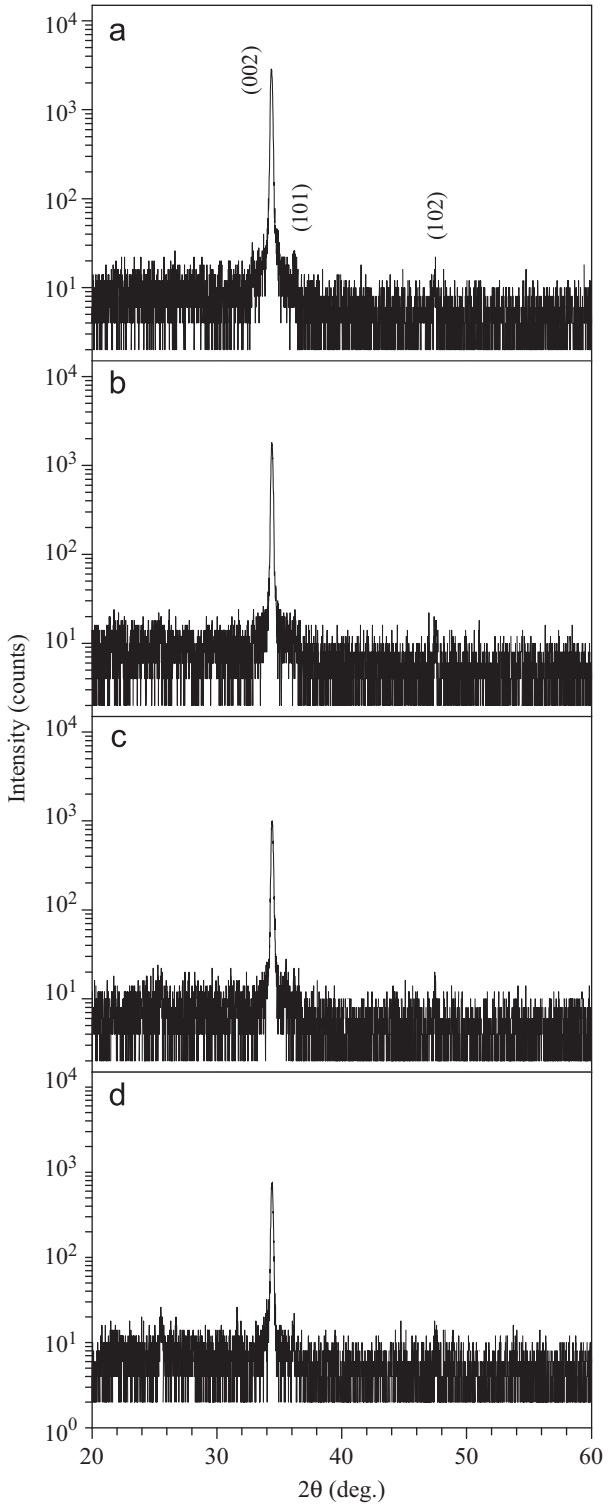

Fig. 1. XRD diffractograms of undoped ZnO annealed at 600 °C for 8 h (a) and B diffusion-doped ZnO samples annealed at 600 °C for 8 h (b), 16 h (c) and 24 h (d).

Fig. 2(a)–(d) shows the XRC data (of the (002) reflections) of the same samples mentioned above. The full width at half-maximum (FWHM) of the curves are determined by fitting

Table 1
Lattice parameters and XRC FWHM for undoped ZnO and B diffusion-doped ZnO samples.

Sample	Lattice parameter c (nm)	FWHM of rocking curve (°)
ZnO annealed at 600 °C for 8 h	0.522	14.5
ZnO:B annealed at 600 °C for 8 h	0.521	15.9
ZnO:B annealed at 600 °C for 16 h	0.521	15.1
ZnO:B annealed at 600 °C for 24 h	0.520	16.7

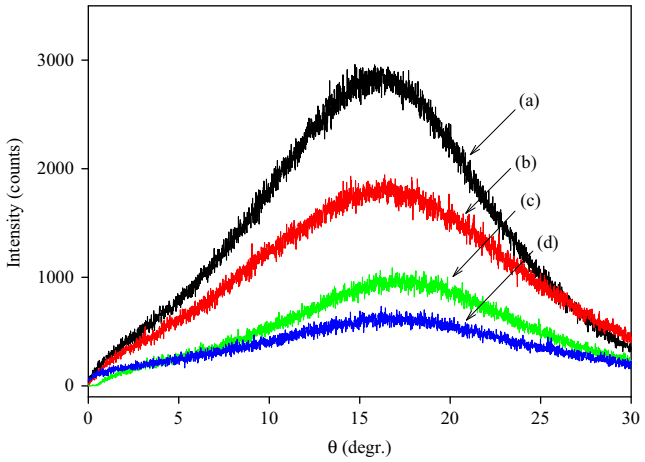

Fig. 2. XRC data for undoped ZnO annealed at 600 °C for 8 h (a) and B diffusion-doped ZnO samples annealed at 600 °C for 8 h (b), 16 h (c) and 24 h (d).

the data with Gaussian functions. The FWHM for the undoped ZnO sample annealed at 600 °C is 14.5°, which indicates a range of crystallite *c*-axis orientations around the normal to the substrate, consistent with the SEM data for the microrod arrays, which shows a range of microrod tilts, as in Fig. 3. The XRC FWHM values of the samples increase after B-doping are summarized in Table 1, indicating that crystal quality/texture is deteriorating with the increase of annealing time for B diffusion-doping samples, which is consistent with the SEM data shown below.

The surface topography of the synthesized ZnO and ZnO:B samples was examined using SEM and the data are shown in Fig. 3. Fig. 3(a) shows the ZnO rod sample annealed at 600 °C for 8 h. This image shows that a dense deposit of reasonably well-aligned hexagonal ZnO microrods is formed, consistent with the XRD data of Figs. 1 and 2, and that the diameter of the ZnO microrods varies from 1 to 2 μm, although some thinner rods with diameters of about 0.5 μm in diameter are occasionally seen. The lengths of the rods are in the order of 3 μm (based on cross sectional SEM data, not shown here). This structure is strongly affected by the B diffusion-doping process as seen in Fig. 3(b). B diffusion and subsequent annealing at 600 °C for 8 h led to a disappearance of the regular shaped rods. In their place, a tubular-shaped microstructure appeared. Diffusional annealing for 16 h resulted in complete alteration of the morphology and a granular microstructure was observed with grain sizes below 1 μm as illustrated in Fig. 3(c). Further increasing the annealing time yielded the microstructures shown in Fig. 3(d) with the grains becoming mostly nano-sized spheres and with some of the grains clustering in addition to the development of some porosity. These data all indicate a deterioration of the crystal quality and these results are consistent with the increase of resistivity observed for the samples annealed at 600 °C for 24 h, as mentioned below. In order to show clearly the effect of the B diffusion process on the samples, the microstructure observed after the 16 h B-diffusion process is shown at a 60° tilt angle in Fig. 3(e).

Fig. 4 shows the XPS survey spectrum of the ZnO:B sample annealed at 600 °C for 24 h, which initially underwent an argon ion sputtering process in order to reduce the concentration of impurity atoms of C and O. Comparing with the known binding energy values of various elements, the survey spectrum indicates the presence of Zn, O, B and C elements in the surface and near-surface regions of the sample as well as Mg, Ca and Na contributions coming from the glass substrate, most likely due to the porosity referred to above which allows some of the substrate to be exposed to the X-ray beam. The inset of Fig. 4 illustrates the core level spectral region of the B 1s peak at approximately 192.6 eV, with the exact peak position corresponding to that for B^{3+} in B_2O_3 (B–O bond) [14,29]. Additionally, the B near surface content of the ZnO:B sample annealed at 600 °C for 24 h was determined from XPS measurements and found to be ~0.8 at%.

The resistivity and electron concentration for undoped ZnO microrods annealed at 600 °C for 8 h are found to be $3.2 \times 10^2\,\Omega\,\text{cm}$ and $2.1 \times 10^{16}\,\text{cm}^{-3}$, respectively. All details relevant to the determination of these values can be found in ref. [30]. However, after B diffusion-doping and subsequent with annealing at 600 °C for 8 h, the resistivity of the samples decreased to a minimum value of 45 Ω cm while the electron concentration reached a maximum value of $1.3 \times 10^{18}\,\text{cm}^{-3}$. This behavior can be explained by the introduction of B^{3+} donor ions to substitutional sites of Zn^{2+} in ZnO host lattice which provides conduction band electrons, leading to an increase in the free carrier concentration [31]. With further increase of the annealing time to 24 h, the resistivity of the samples reaches $3.3 \times 10^2\,\Omega\,\text{cm}$ and the carrier concentration decreased to $5.4 \times 10^{17}\,\text{cm}^{-3}$, as listed in Table 2. The decrease in the carrier concentration most probably results from the increased B concentration generating intrinsic defects which compensate some of the B donors, which reduces the carrier concentration. The increase in resistivity may also be related to the increased porosity with increasing annealing time (shown in Fig. 3(d)) reducing the carrier mobility.

In order to investigate the influence of B diffusion doping on optical emission and defect formation, PL spectra of all the samples were measured at 10 K. Fig. 5(a)–(d) shows PL

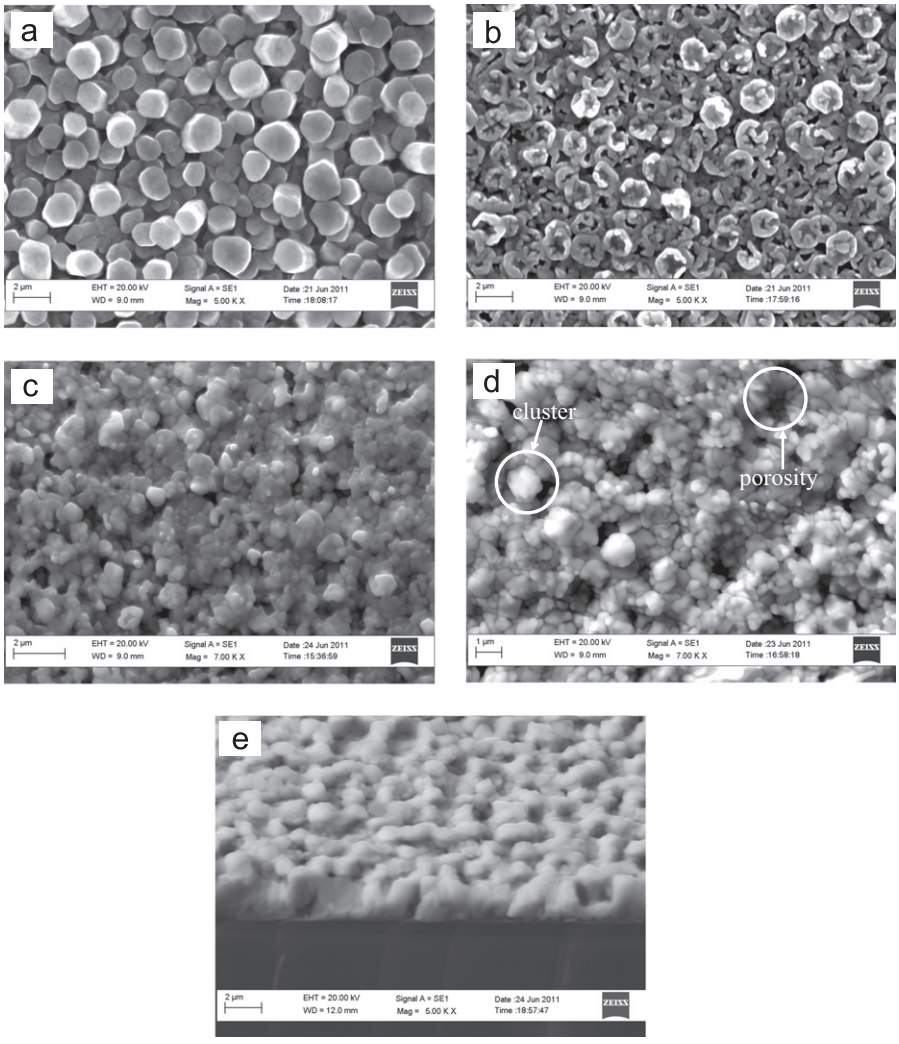

Fig. 3. SEM images of undoped ZnO annealed at 600 °C for 8 h (a) and B diffusion-doped ZnO samples annealed at 600 °C for 8 h (b), 16 h (c), 24 h (d) and a 60° tilted view of a B diffusion-doped ZnO sample annealed at 600 °C for 16 h (e).

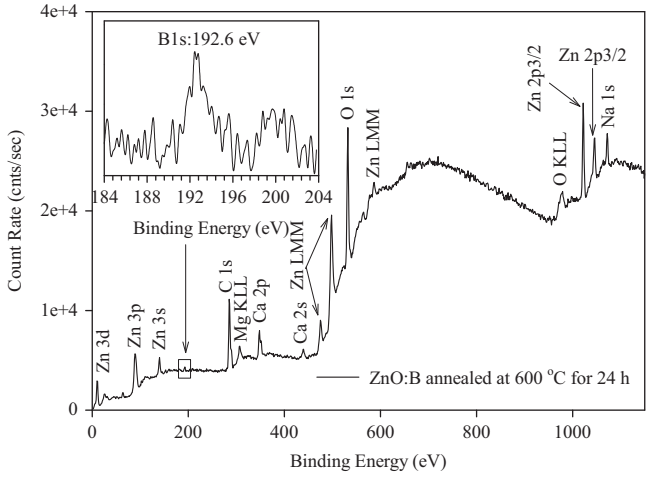

Fig. 4. XPS survey spectrum for B diffusion-doped ZnO sample annealed at 600 °C for 24 h. The inset corresponds to the B 1s core level.

spectra of undoped ZnO annealed at 600 °C for 8 h and B diffusion-doped ZnO samples annealed at 600 °C for 8, 16 and 24 h, respectively (all spectra normalized to the strongest near band edge UV peak emission). The dominant UV peak seen in all the samples is located at ~3.36 eV and is ascribed to the near band edge (NBE) emission due to excitons bound to donors (D^0X, members of the so-called I line series) [32]. The energies of these peaks are identical within less than 10 meV for all samples, indicating that the dominant donor bound exciton emission energy is not significantly affected by the B incorporation and thus that the band gaps at low temperatures in all samples are almost identical. Any slight changes in the peak emission are ascribed to changes in the dominant donor following boron incorporation. The inset of the Fig. 5 shows, on a magnified scale, the relative deep level visible band emission (DLE) of undoped ZnO annealed at 600 °C for 8 h and ZnO:B samples annealed at 600 °C for 8 h. These data display an

Table 2
Carrier concentration and resistivity values of undoped ZnO and B diffusion-doped ZnO samples.

Sample	Carrier concentration (cm^{-3})	Resistivity (Ω cm)
ZnO annealed at 600 °C for 8 h	2.1×10^{16}	3.2×10^{2}
ZnO:B annealed at 600 °C for 8 h	1.3×10^{18}	4.5×10^{1}
ZnO:B annealed at 600 °C for 24 h	5.4×10^{17}	3.3×10^{2}

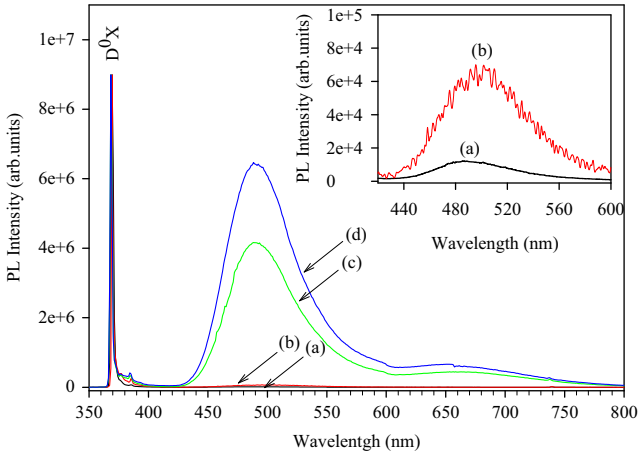

Fig. 5. Low temperature PL spectra of undoped ZnO annealed at 600 °C for 8 h (a), and B diffusion-doped ZnO samples annealed at 600 °C for 8 h (b), 16 h (c), 24 h (d). Inset shows DLE band on a magnified intensity scale for the samples shown labeled (a) and (b).

increase in the relative intensity of DLE with B diffusion-doping, suggesting that both B diffusion-doping and annealing in argon ambient have an effect on the DLE band intensity. It is usually believed that annealing in O-deficient conditions such as argon and/or vacuum helps to form point defects in ZnO [33]. There are also likely to be effects from B incorporation into Zn sites and hence there may be complexing of B with native defects like oxygen vacancies (V_o), zinc vacancies (V_{Zn}) or oxygen interstitials (O_i) [34]. Additionally, as shown in Fig. 5, with a further increase of annealing time, the samples display a significant increase in the intensity of the DLE (in the range of 425–600 nm), implying a significant increase of the concentrations of the intrinsic defects responsible such as V_{Zn}, V_o and Zn_i [35,36]. Yu et al. investigated the effects of B concentration on ZnO nanorods grown by a low-temperature hydrothermal reaction method on Si substrates and found that the relative intensity of the broad visible emission increased with an increase of B doping content from 0 at% to 3 at%. They proposed that the ZnO lattice becomes more distorted for higher doping levels and that the defect density due to vacancies, oxygen, and/or dangling bonds would be enhanced, resulting in a stronger visible emission [37]. This explanation is consistent with our observations of increased strain in these samples measured by XRD. In addition, at longer wavelengths, B diffusion-doped ZnO samples annealed at 600 °C for 16 and 24 h exhibit a broad red luminescence in the range 610–800 nm which is probably due to (O_i) defects [38–41].

In order to understand the magnetic behavior of the undoped and B diffusion-doped ZnO samples, the magnetization versus field dependence curves of these samples were measured at 300 K and are shown in Fig. 6. The diamagnetic contribution from the substrate is subtracted from the total magnetization. Undoped ZnO microrods annealed at 600 °C for 8 h (shown in inset) did not exhibit ferromagnetic behavior at room temperature. Similar diamagnetic behavior was observed by Liu et al. for ZnO nanowires grown by a vapor phase transport process [12]. On the other hand, B-doped ZnO films annealed at 600 °C for both 8 and 24 h are found to show hysteresis, indicating ferromagnetic behavior at room temperature. The ZnO:B samples annealed at 600 °C for 8 and 24 h possess a saturation magnetization (M_s) value of 0.89 and 0.45 emu/cm^3, respectively, indicating a decrease in the ferromagnetism with an increase of annealing time. It is generally believed that there is a positive relation between the value of M_s and the carrier concentration of the samples, suggesting that the decrease of carrier concentration may help to reduce the ferromagnetic response of the material [42]. Thus one of the reasons for the deterioration of the ferromagnetic response may be due to the decrease of carrier concentration with increase of annealing time for ZnO:B samples. The other reason may be the increased intrinsic defect concentrations introduced during the annealing process as discussed earlier. A very similar result was obtained by Sharma et al. who investigated the effect of hydrogenation time on magnetic properties for hydrogenated Mn-doped ZnO prepared by a solid state reaction method, which showed that as the hydrogenation time increased from 3 h to 5 h, the ferromagnetic response deteriorated due to defects introduced in the samples for longer hydrogenation times [43]. It is also showed that (O_i)

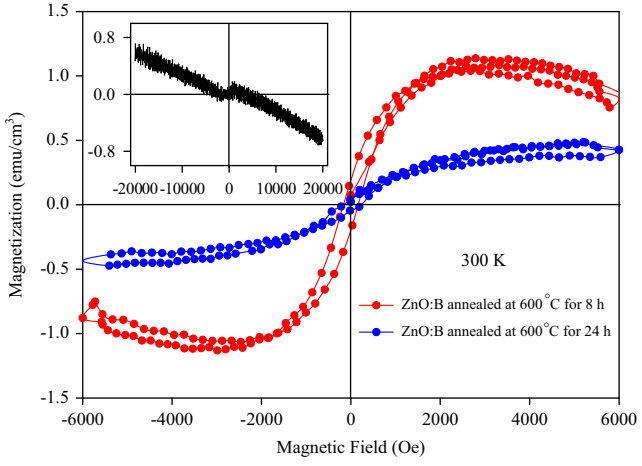

Fig. 6. Room temperature M–H curves of B diffusion-doped ZnO samples annealed at 600 °CC for 8 h and 24 h. Inset shows M–H curve of undoped ZnO microrods annealed at 600 °C for 8 h.

defects in particular have an important effect leading to the decrease of ferromagnetic response and therefore this may especially affect our ZnO:B sample annealed at 600 °C for 24 h which exhibited poorer magnetic behavior than the ZnO:B sample annealed at 600 °C for 8 h and which showed evidence in the PL data discussed earlier for the presence of O_i defects [41].

With regard to the origin of the ferromagnetism observed in our samples and considering the full range of XRD, XPS, electrical and optical measurements, our data support the hypothesis that the observed room temperature ferromagnetic behavior is related to the presence of intrinsic defects in addition to the B dopant. We have not observed B and B-related oxides in our XRD data, but even if these are present below the sensitivity limit of our equipment, the fact that these phases are nonmagnetic means that the origin of ferromagnetism in these samples cannot be attributed to these impurity phases. As discussed in relation to the PL data previously, the relative intensity of the deep level band for B diffusion-doped ZnO samples is higher than that for undoped ZnO, indicating that boron-doping may increase the concentration of intrinsic defects such as V_{Zn}, V_o and Zn_i which may play significant roles to induce the room temperature ferromagnetism for ZnO:B samples [44].

Our theoretical calculations support these conclusions from experiments. The calculated lattice parameters for wurtzite ZnO yield values of $a=0.3253$ nm and $c/a=1.611$ within the GGA-PBE approximation, which are in good agreement with experimental data [45]. The 100′s of nm/μm-scale morphology of the ZnO deposits in our experiments mean that carrier confinement and other effects due to low dimensionality are not relevant and calculation methods for bulk ZnO material are suitable for comparison with these samples. In order to model the B doping process we have substituted two Zn atoms in the 128 atom ($4\times4\times2$) supercell of ZnO by B atoms, which corresponds to the doping concentration of 3.12 at%. We have studied the magnetic properties of $Zn_{1-x}B_xO$, with no other defects, which is found to be nonmagnetic. However, as highlighted above, defects in semiconductors can play an important role with respect to electronic and magnetic properties of the system. Therefore, we have chosen to investigate intrinsic defects situated in B-doped ZnO. We have considered two types of defects in the system: the oxygen vacancy (V_o) and the Zn-vacancy (V_{Zn}). Two Zn or O atoms are removed from supercell, respectively, to model these scenarios and the corresponding vacancy concentration is 3.12 at%.

Firstly, we have investigated the magnetic properties of B-doped ZnO with V_o, a system which is still nonmagnetic. V_o does not induce a magnetic moment in the neighboring atoms of the vacancy. Secondly we have introduced V_{Zn} defects in the system to explore the magnetic moment in the B-doped ZnO. We have assumed two V_{Zn} defects in the bulk with the distance 0.548 nm between these vacancies. Here, we have considered two cases. In case-I, we have put the dopant at the distance of 0.313 nm from the Zn-vacancy and in second case, distance between dopant and vacancy is 0.548 nm. It is observed that the ferromagnetic (FM) phase is more stable than the antiferromagnetic (AFM) phase by an energy difference of 278 and 177 meV for case-I and case-II, respectively. This energy difference in B-doped ZnO with V_{Zn} defects is very high compared to the thermal energy at or below room temperature and is certainly enough to justify room temperature ferromagnetism. The total magnetic moment of the FM phase is 1.48 μ_B. We have calculated the spin polarized total and partial density of states (PDOS) of Zn, O and B atoms which are in neighboring sites to V_{Zn} defects in the system (shown in Fig. 7). This clearly indicates that the induced magnetic moments are mainly contributed by oxygen atoms (0.166 μ_B) which are very close to the nearest neighbor sites to B–Zn vacancy pairs, while the neighboring Zn atoms carry very small magnetic moments (around 0.027 μ_B). The partially filled states appear in the partial density of states of O which is very close to the B and Zn vacancy. Neighboring Zn 3d and O 2p states of the V_{Zn} are hybridized at the Fermi level. The density of states indicates that the system shows half metallic behavior which decreases the resistivity of the B-ZnO system with V_{Zn} defects.

The magnetization versus temperature (M–T) curves were measured in a temperature range of 20–300 K for ZnO:B samples annealed at 600 °C for 8 h and 24 h and are shown in Fig. 8. As can be seen from these data, the magnetization of both curves is almost constant in the temperature range 50–300 K followed by an abrupt increase upon further cooling toward 20 K. Based on these data we can conclude that the Curie temperatures for these samples are well above room temperature, but it is hard to determine the exact value as it exceeds the accessible range of our measurements.

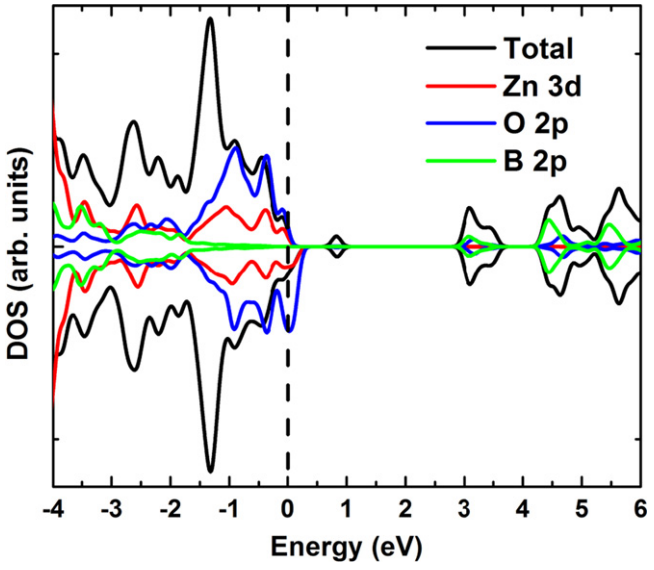

Fig. 7. Calculated total and partial density of states of B-doped ZnO with Zn-vacancy defects. The vertical line indicates the Fermi level.

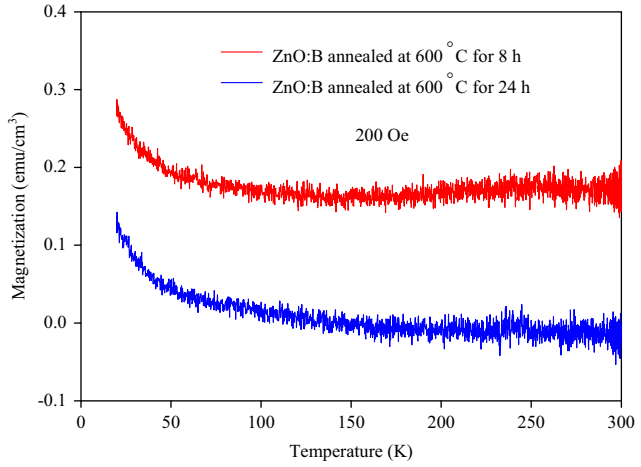

Fig. 8. Temperature dependence of magnetization of B diffusion-doped ZnO samples annealed at 600 °C for 8 h and 24 h.

4. Conclusions

Based on the data from morphological, structural, electrical, optical, and magnetic measurements of our samples the following main points emerge: (i) both ZnO and ZnO:B samples have the wurtzite structure with *c*-axis textured normal to the substrate surface; (ii) boron incorporation leads to substantial changes in the ZnO microstructure; (iii) XPS results reveal the incorporation of B as B^{3+} on Zn sites in the ZnO host lattice; (iv) Hall measurements show that the carrier concentration increased from 2.1×10^{16} cm^{-3} to 1.3×10^{18} cm^{-3} and 5.4×10^{17} cm^{-3} for ZnO annealed at 600 °C for 8 h and ZnO:B samples annealed at 600 °C for 8 and 24 h, respectively; (v) PL results show that boron doping increases the relative intensity of deep level intrinsic defect-related emission bands; (vi) B diffusion-doped ZnO samples clearly displayed FM loops at room temperature and (based both on the experimental data and first principles theoretical predictions) the origin of the observed room temperature FM is concluded to be due to oxygen atoms in the nearest neighbor sites to B–Zn vacancy pairs, consistent with the conclusions of Xu et al. [14].

Acknowledgments

SY gratefully acknowledges the support of the Council of Turkish Higher Education in the form of a fellowship to support extended visits to foreign institutions. This work was also supported by the research fund of Karadeniz Technical University, Trabzon, Turkey, under Contract no. 2010.111.001.3. EMcG gratefully acknowledges support from the Science Foundation Ireland Strategic Research Cluster grant entitled "Functional Oxides and Related Materials for Electronics" (FORME). Additionally, we would like to acknowledge the Swedish Research Council (under the projects VR and FORMAS) for financial support. SNIC and UPPMAX are acknowledged for providing computing time. JN is thankful to the Higher Education Commission (HEC) of Pakistan.

References

[1] W.Z. Xu, Z.Z. Ye, Y.J. Zeng, L.P. Zhu, B.H. Zhao, L. Jiang, J.G. Lu, H.P. He, S.B. Zhang, ZnO light-emitting diode grown by plasma-assisted metal organic chemical vapor deposition, Applied Physics Letters 88 (2006) 173506–173508.
[2] Z.G. Yang, L.P. Zhu, Y.M. Guo, W. Tian, Z.Z. Ye, B.H. Zhao, Valence-band offset of p-NiO/n-ZnO heterojunction measured by X-ray photoelectron spectroscopy, Physics Letters A 375 (2011) 1760–1763.
[3] C. Leach, N.K. Ali, D. Cupertino, R. Freer, Microwave-assisted sintering of ZnO varistors: Local microstructure and functional property variations, Materials Science and Engineering B 170 (2010) 15–21.
[4] V. Bhosle, A. Tiwari, J. Narayan, Electrical properties of transparent and conducting Ga doped ZnO, Journal of Applied Physics 100 (2006) 033713–033718.
[5] W.W. Wenas, A. Yamada, K. Takahashi, M. Yoshino, M. Konagai, Electrical and optical properties of boron-doped ZnO thin films for solar cells grown by metalorganic chemical vapor deposition, Journal of Applied Physics 70 (1991) 7119–7123.
[6] T. Dietl, H. Ohno, F. Matsukura, J. Cibert, D. Ferrand, Zener model description of ferromagnetism in zinc-blende magnetic semiconductors, Science 287 (2000) 1019–1022.
[7] K. Ueda, H. Tabata, T. Kawai, Magnetic and electric properties of transition-metal-doped ZnO films, Applied Physics Letters 79 (2001) 988–990.
[8] X.X. Liu, F.T. Lin, L.L. Sun, W.J. Cheng, X.M. Ma, W.Z. Shi, Doping concentration dependence of room-temperature ferromagnetism for Ni-doped ZnO thin films prepared by pulsed-laser deposition, Applied Physics Letters 88 (2006) 062508–062510.
[9] A.K. Pradhan, K. Zhang, S. Mohanty, J.B. Dadson, D. Hunter, High-temperature ferromagnetism in pulsed-laser deposited epitaxial (Zn,Mn)O thin films: effects of substrate temperature, Applied Physics Letters 86 (2005) 152511–152513.
[10] H. Pan, J.B. Yi, L. Shen, R.Q. Wu, J.H. Yang, J.Y. Lin, Y.P. Feng, J. Ding, L.H. Van, J.H. Yin, Room-temperature ferromagnetism in carbon-doped ZnO, Physical Review Letters 99 (2007) 127201–127204.
[11] X.J. Ye, H.A. Song, W. Zhong, M.H. Xu, X.S. Qi, C.Q. Jin, Z.X. Yang, C.T. Au, Y.W. Du, The effect of nitrogen incorporation on the magnetic properties of carbon-doped ZnO, Journal of Physics D: Applied Physics 41 (2008) 155005–155008.
[12] K.W. Liu, M. Sakurai, M. Aono, Indium-doped ZnO nanowires: optical properties and room-temperature ferromagnetism, Journal of Applied Physics 108 (2010) 043516–043520.
[13] K.Y. Wu, Q.Q. Fang, W.N. Wang, C. Zhou, W.J. Huang, J.G. Li, Q.R. Lv, Y.M. Liu, Q.P. Zhang, H.M. Zhang, Influence of nitrogen on the defects and magnetism of ZnO:N thin films, Journal of Applied Physics 108 (2010) 063530–063534.
[14] X.G. Xu, H.L. Yang, Y. Wu, D.L. Zhang, S.Z. Wu, J. Miao, Y. Jiang, X.B. Qin, X.Z. Cao, B.Y. Wang, Intrinsic room temperature ferromagnetism in boron-doped ZnO, Applied Physics Letters 97 (2010) 232502–232504.
[15] T.S. Herng, S.P. Lau, C.S. Wei, L. Wang, B.C. Zhao, M. Tanemura, Y. Akaike, Stable ferromagnetism in p-type carbon-doped ZnO nanoneedles, Applied Physics Letters 95 (2009) 133103–133105.
[16] X.B. Wang, D.M. Li, F. Zeng, F. Pan, Microstructure and properties of Cu-doped ZnO films prepared by dc reactive magnetron sputtering, Journal of Physics D: Applied Physics 38 (2005) 4104–4108.
[17] Z.X. Cheng, X.L. Wang, S.X. Dou, K. Ozawa, H. Kimura, P. Munroe, Fabrication, Raman spectra and ferromagnetic properties of the transition metal doped ZnO nanocrystals, Journal of Physics D: Applied Physics 40 (2007) 6518–6521.

[18] X. Peng, R. Ahuja, Non-transition-metal doped diluted magnetic semiconductors, Applied Physics Letters 94 (2009) 102504–102506.
[19] J.M.D. Coey, A.P. Douvalis, C.B. Fitzgerald, M. Venkatesan, Ferromagnetism in Fe-doped SnO_2 thin films, Applied Physics Letters 84 (2004) 1332–1334.
[20] S. Yılmaz, E. McGlynn, E. Bacaksız, Ş. Özcan, D. Byrne, M.O. Henry, R.K. Chellappan, Effects of Cu diffusion-doping on structural, optical, and magnetic properties of ZnO nanorod arrays grown by vapor phase transport method, Journal of Applied Physics 111 (2012) 013903–013909.
[21] S. Yılmaz, M. Parlak, Ş. Özcan, M. Altunbaş, E. McGlynn, E. Bacaksız, Structural, optical and magnetic properties of Cr doped ZnO microrods prepared by spray pyrolysis method, Applied Surface Science 257 (2011) 9293–9298.
[22] P.E. Blochl, Projector augmented-wave method, Physical Review B 50 (1994) 17953–17979.
[23] G. Kresse, J. Hafner, Ab initio molecular-dynamics simulation of the liquid-metal-amorphous-semiconductor transition in germanium, Physical Review B 49 (1994) 14251–14269.
[24] G. Kresse, D. Joubert, From ultrasoft pseudopotentials to the projector augmented-wave method, Physical Review B 59 (1999) 1758–1775.
[25] J.P. Perdew, J.A. Chevary, S.H. Vosko, K.A. Jackson, M.R. Pederson, D.J. Singh, C. Fiolhais, Atoms, molecules, solids, and surfaces: applications of the generalized gradient approximation for exchange and correlation, Physical Review B 46 (1992) 6671–6687.
[26] J.P. Perdew, Y. Wang, Accurate and simple analytic representation of the electron-gas correlation energy, Physical Review B 45 (1992) 13244–13249.
[27] H.J. Monkhorst, J.D. Pack, Special points for Brillouin-zone integrations, Physical Review B 13 (1976) 5188–5192.
[28] H. Deng, J.J. Russell, R.N. Lamb, B. Jiang, Microstructure control of ZnO thin films prepared by single source chemical vapor deposition, Thin Solid Films 458 (2004) 43–46.
[29] J. Hu, R.G. Gordon, Deposition of boron doped zinc oxide films and their electrical and optical properties, Journal of the Electrochemical Society 139 (1992) 2014–2022.
[30] E. Bacaksiz, S. Aksu, G. Çankaya, S. Yılmaz, İ. Polat, T. Küç ükömeroğlu, A. Varilci, Fabrication of p-type CuSCN/n-type microstructured ZnO heterojunction structures, Thin Solid Films 519 (2011) 3679–3685.
[31] G. Kim, J. Bang, Y. Kim, S.K. Rout, S.I. Woo, Structural, electrical and optical properties of boron doped ZnO thin films using LSMCD method at room temperature, Applied Physics A 97 (2009) 821–828.
[32] B.K. Meyer, H. Alves, D.M. Hofmann, W. Kriegseis, D. Forster, F. Bertram, J. Christen, A. Hoffmann, M. Straßburg, M. Dworzak, U. Haboeck, A.V. Rodina, Bound exciton and donor–acceptor pair recombinations in ZnO, Physica Status Solidi B 241 (2004) 231–260.
[33] Y. Du, F. Zeng, Annealing effects on the cathodoluminescence properties of individual ZnO nanowire, Materials Letters 65 (2011) 2238–2240.
[34] Z.Q. Chen, M. Maekawa, A. Kawasuso, S. Sakai, H. Naramoto, Annealing process of ion-implantation-induced defects in ZnO: chemical effect of the ion species, Journal of Applied Physics 99 (2006) 093507–093511.
[35] M. Chen, Z. Wang, D. Han, F. Gu, G. Guo, Porous ZnO polygonal nanoflakes: synthesis, use in high-sensitivity NO_2 gas sensor, and proposed mechanism of gas sensing, Journal of Physical Chemistry C 115 (2011) 12763–12773.
[36] Ü. Özgür, Y.I. Alivov, C. Liu, A. Teke, M.A. Reshchikov, S. Dogan, V. Avrutin, S.J. Cho, H. Morkoc, A comprehensive review of ZnO materials and devices, Journal of Applied Physics 98 (2005) 041301–041403.
[37] Q. Yu, L. Li, H. Li, S. Gao, Da. Sang, J. Yuan, P. Zhu, Synthesis and properties of boron doped ZnO nanorods on silicon substrate by low-temperature hydrothermal reaction, Applied Surface Science 257 (2011) 5984–5988.
[38] S.A. Studenikin, N. Golego, M. Cocivera, Fabrication of green and orange photoluminescent, undoped ZnO films using spray pyrolysis, Journal of Applied Physics 84 (1998) 2287–2294.
[39] L. Cui, H.Y. Zhang, G.G. Wang, F.X. Yang, X.P. Kuang, R. Sun, J.C. Han, Effect of annealing temperature and annealing atmosphere on the structure and optical properties of ZnO thin films on sapphire (0001) substrates by magnetron sputtering, Applied Surface Science 258 (2012) 2479–2485.
[40] W.W. Li, W.L. Yu, Y.J. Jiang, C.B. Jing, J.Y. Zhu, M. Zhu, Z.G. Hu, X.D. Tang, J.H. Chu, Structure, optical, and room-temperature ferromagnetic properties of pure and transition-metal-(Cr, Mn, and Ni)-doped ZnO nanocrystalline films grown by the sol–gel method, Journal of Physical Chemistry C 114 (2010) 11951–11957.
[41] W. Liu, W. Li, Z. Hu, Z. Tang, X. Tang, Effect of oxygen defects on ferromagnetic of undoped ZnO, Journal of Applied Physics 110 (2011) 013901–013905.
[42] K. Potzger, A. Shalimov, S. Zhou, H. Schmidt, A. Mücklich, M. Helm, J. Fassbender, M. Liberati, E. Arenholz, Amorphous clusters in Co implanted ZnO induced by boron preimplantation, Journal of Applied Physics 105 (2009) 123917–123924.
[43] V.K. Sharma, G.D. Varma, Oxygen vacancies induced room temperature ferromagnetism in hydrogenated Mn-doped ZnO, Journal of Applied Physics 102 (2007) 056105–056107.
[44] J.M.D. Coey, M. Venkatesan, C.B. Fitzgerald, Donor impurity band exchange in dilute ferromagnetic oxides, Nature Materials 4 (2005) 173–179.
[45] R.R. Reeber, Lattice parameters of ZnO from 4.2° to 296°K, Journal of Applied Physics 41 (1970) 5063–5066.